

Probing the Transition State with Negative Ion Photodetachment: The Cl + HCl and Br + HBr Reactions

R. B. Metz,[†] A. Weaver,[‡] S. E. Bradforth,[§] T. N. Kitsopoulos, and D. M. Neumark^{*||}

Department of Chemistry, University of California, Berkeley, California 94720 (Received: June 29, 1989)

The transition-state region for neutral hydrogen-transfer reactions can be probed by photodetaching the appropriate stable, hydrogen-bonded negative ion. This paper presents a detailed account of this method, in which the Cl + HCl and Br + HBr reactions are investigated by photoelectron spectroscopy of ClHCl⁻, BrHBr⁻, and the corresponding deuterated species. The photoelectron spectra exhibit resolved vibrational structure attributed to the unstable neutral [ClHCl] or [BrHBr] complex. The peaks in the spectra are assigned to the antisymmetric stretch mode of the complex, and the peak widths are sensitive to the lifetime of the complex. The BrHBr⁻ and BrDBr⁻ spectra exhibit narrow (15–20 meV) peaks that are likely to result from reactive resonance states supported by the Br + HBr potential energy surface, as well as peaks that appear to be from an electronically excited state of the [BrHBr] complex. The BrHBr⁻ and BrDBr⁻ results have been analyzed to yield an "effective" collinear potential energy surface for the Br + HBr reaction.

Introduction

One of the fundamental issues in the field of reaction dynamics is the nature of the transition state in a chemical reaction. The features of a reactive potential energy surface near the transition state affect nearly all of the important properties of a chemical reaction including the rate constant, the effect of reactant translational and internal energy on reactivity, and the product energy and angular distribution. The aim of much of state-to-state chemistry over the last 10–15 years has been to measure these asymptotic properties as accurately and completely as possible and to attempt to use this information to learn about the region of the potential energy surface in the vicinity of the transition state (the transition-state region). While state-to-state scattering experiments have led to a qualitative understanding of reactive potential energy surfaces,¹ averaging over reactant orientation and impact parameter in most of these experiments greatly complicates the extraction of transition-state properties from the measured asymptotic distributions. The transition-state region is, in principle, amenable to study by quantum chemistry calculations, but the ab initio construction of a potential energy surface is difficult even for the simplest chemical reactions.²

This situation has motivated the development of a series of "transition state spectroscopy" experiments^{3,4} designed to probe the transition-state region itself rather than the asymptotic properties of a reactive encounter. The initial experiments in this field were performed by Polanyi,⁵ Brooks,⁶ and their co-workers. The transition-state region of several reactive and dissociative systems has since been studied in a variety of "full collision"^{7–9} and "half collision"^{10–12} experiments. Recent experiments in this area of particular interest include the work of Nieh and Valentini¹³ on the H + H₂ reaction, in which the observation of quasi-bound states of the [H₃] complex was reported, and the real-time studies of photodissociation by Zewail and co-workers.¹⁴

We have devised and implemented a transition-state spectroscopy experiment in which negative ion photodetachment is used to probe the transition-state region for a neutral bimolecular reaction. Our experiment draws on earlier studies in which photodetachment of a stable negative ion generated an unstable neutral species. These include total photodetachment cross section measurements by Golub and Steiner¹⁵ on (H₂O)OH⁻ and, more recently, by Brauman and co-workers on a series of ions ROHF⁻.¹⁶ In these studies, photodetachment of a stable, hydrogen-bonded ion produced a neutral complex unstable with respect to dissociation. In another important experiment, Lineberger and co-workers¹⁷ measured the photoelectron spectrum of the vinylidene anion C₂H₂⁻. Photodetachment of this anion produces the vi-

nylidene radical, which isomerizes rapidly to acetylene. Nonetheless, the negative ion photoelectron spectrum shows vibrational structure associated with the unstable form of the radical.

In our experiments, the transition-state region of the heavy plus light-heavy reaction X + HY → HX + Y is probed by laser photoelectron spectroscopy of the stable hydrogen-bonded negative ion XHY⁻. This provides a direct, spectroscopic probe of the [XHY] collision complex, as long as the geometry of the ion is similar to that of the neutral transition state. Figure 1 shows a one-dimensional idealization of our experiment for a symmetric exchange reaction (X = Y). The potential energy of the ion and neutral are shown as a function of an appropriate reaction coordinate. The [XHX] complex formed at or near the top of the barrier is unstable with respect to motion along the reaction coordinate. However, the barrier is actually a saddle point on a multidimensional potential energy surface. The XHX⁻ photoelectron spectrum can therefore exhibit peaks that correspond to vibrational motion along coordinates "perpendicular" to the reaction coordinate. The peak spacings yield the frequencies associated with these vibrations, while the peak widths are an in-

(1) Levine, R. D.; Bernstein, R. B. *Molecular Reaction Dynamics and Chemical Reactivity*; Oxford University Press: New York, 1987; pp 396–510.

(2) Siegbahn, P.; Liu, B. *J. Chem. Phys.* **1978**, *68*, 2457. Truhlar, D. G.; Horowitz, C. J. *J. Chem. Phys.* **1978**, *68*, 2468. Schaefer, H. F., III. *J. Phys. Chem.* **1985**, *89*, 5336. Schwenke, D. W.; Steckler, R.; Brown, F. B.; Truhlar, D. G. *J. Chem. Phys.* **1986**, *84*, 5706.

(3) Brooks, P. R. *Chem. Rev.* **1988**, *88*, 407.

(4) Zewail, A. H. *Science* **1988**, *242*, 1645.

(5) Arrowsmith, P.; Bartoszek, F. E.; Bly, S. H. P.; Carrington, T., Jr.; Charters, P. E.; Polanyi, J. C. *J. Chem. Phys.* **1980**, *73*, 5895.

(6) Hering, P.; Brooks, P. R.; Curl, R. F., Jr.; Judson, R. S.; Lowe, R. S. *Phys. Rev. Lett.* **1980**, *44*, 687. Maguire, T. C.; Brooks, P. R.; Curl, R. F.; Spence, J. H.; Ulvick, S. J. *J. Chem. Phys.* **1986**, *85*, 844.

(7) Grieneisen, H. P.; Xue-jing, H.; Kompa, K. L. *Chem. Phys. Lett.* **1981**, *82*, 421.

(8) Kleiber, P. D.; Lyyra, A. M.; Sando, K. M.; Zafirooulos, V.; Stwalley, W. C. *J. Chem. Phys.* **1986**, *85*, 5493.

(9) Benz, A.; Morgner, H. *Mol. Phys.* **1986**, *57*, 319.

(10) Buelow, S.; Radhakrishnan, G.; Catanzarite, J.; Wittig, C. *J. Chem. Phys.* **1985**, *83*, 444.

(11) Imre, D. G.; Kinsey, J. L.; Field, R. W.; Katayama, D. H. *J. Phys. Chem.* **1982**, *86*, 2564.

(12) Breckenridge, W. H.; Jouvot, C.; Soep, B. *J. Chem. Phys.* **1986**, *84*, 1443.

(13) Nieh, J.-C.; Valentini, J. J. *Phys. Rev. Lett.* **1988**, *60*, 519.

(14) Dantus, M.; Rosker, M. J.; Zewail, A. H. *J. Chem. Phys.* **1987**, *87*, 2395. Bowmam, R. M.; Dantus, M.; Zewail, A. H. *Chem. Phys. Lett.* **1989**, *156*, 131.

(15) Golub, S.; Steiner, B. *J. Chem. Phys.* **1968**, *49*, 5191.

(16) Moylan, C. R.; Dodd, J. A.; Han, C.; Brauman, J. I. *J. Chem. Phys.* **1987**, *86*, 5350.

(17) Burnett, S. M.; Stevens, A. E.; Feigerle, C. S.; Lineberger, W. C. *Chem. Phys. Lett.* **1982**, *100*, 124. Ervin, K. M.; Ho, J.; Lineberger, W. C., submitted for publication in *J. Chem. Phys.*

[†]NSF Predoctoral Fellow.

[‡]NSERC (Canada) Postgraduate Scholar.

[§]University Fellow, University of California.

^{||}NSF Presidential Young Investigator and Alfred P. Sloan Fellow.

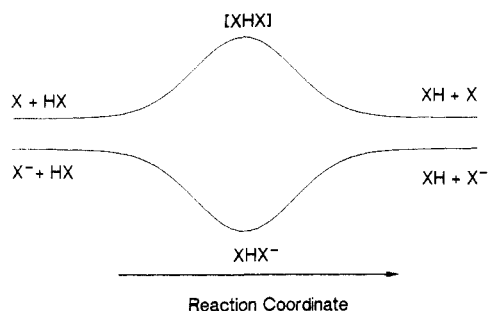


Figure 1. Schematic potentials along the reaction coordinate for $X + HX$ and $X^- + HX$.

dication of motion along the reaction coordinate; the ratio of peak spacing to peak widths measures how many vibrations the complex undergoes as it dissociates. We therefore learn about the spectroscopy and dissociation dynamics of the collision complex.

X and Y can be atomic or polyatomic species. The simplest systems are symmetric reactions of the type $X + HX \rightarrow XH + X$, where X is a halogen atom. This paper covers two such reactions: the $Cl + HCl$ and $Br + HBr$ reactions. We have also successfully applied this technique to cases where X and Y are two unlike halogen atoms, as well as to more complex systems such as $X = F$ and $Y = CH_3O$ and C_2H_5O .¹⁸ These results will be discussed in detail in a future publication.

Consider the reaction $Cl + HCl \rightarrow HCl + Cl$, which we study by photodetaching $ClHCl^-$. Rate constants have been measured for this reaction,¹⁹ and ab initio calculations on the neutral potential energy surface have been performed.²⁰ On the basis of these studies, the reaction is believed to proceed along a collinear or nearly collinear minimum energy path with a barrier of ~ 8 kcal/mol. The calculated interchlorine distance at the saddle point is 2.94 Å. The high-resolution infrared spectrum of gas-phase $ClHCl^-$,²¹ in conjunction with recent ab initio calculations²² and earlier matrix isolation studies,²³ indicates that the ion is linear and centrosymmetric with an equilibrium interchlorine distance of 3.1122 Å. Photodetachment of the ion, a vertical process, should therefore access the transition-state region of the $Cl + HCl$ potential energy surface. There is no kinetic or scattering data available on the $Br + HBr$ reaction, nor have any high-level ab initio calculations been performed. Nonetheless, we expect that photodetachment of $BrHBr^-$ should allow us to probe the transition-state region for the corresponding reaction.

Our experiment probes the transition state under well-defined conditions. Photodetaching the $ClHCl^-$ ion initiates the reaction on the $Cl + HCl$ surface with all three atoms essentially collinear, and the averaging over reactant orientation that occurs in most scattering experiments is largely eliminated. Because the ejected electron is so light, the ion and neutral complex have approximately the same angular momentum. One can therefore limit the total angular momentum of the complex by performing the experiment with rotationally cold ions. This is in sharp contrast to a scattering experiment in which there is no control over reactant impact parameter and thus the total angular momentum.

A key feature of our experiment is the ability to test an interesting theoretical prediction concerning $X + HX$ reactions: the

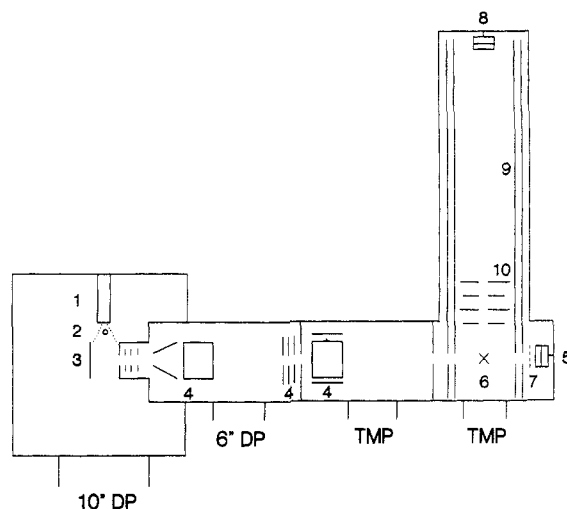


Figure 2. Schematic diagram of the time-of-flight photoelectron spectrometer. See the text for a description.

existence of long-lived reactive resonance states.²⁴ Collinear quantum reactive scattering calculations on model potential energy surfaces for $X + HX$ reactions^{25,26} show sharp resonance structure in the reaction probability as a function of energy. This is superimposed on a smoothly varying background due to direct scattering. The sharp structure is attributed to long-lived vibrationally excited states of the collision complex localized near the transition state. The resonances have widths of about 1 cm^{-1} (0.12 meV), indicating lifetimes in the range of several picoseconds for these states. Three-dimensional calculations on the $Cl + HCl$ reaction also show resonance structure in the total reaction cross section,²⁷ although the resonances are broader (5 meV) and less pronounced relative to the contribution from direct scattering than in the two-dimensional calculations.

With reference to Figure 1, one can think of resonances as arising from states of the collision complex that are not only bound along directions perpendicular to the reaction coordinate, but are also quasi-bound along the reaction coordinate. These states can lead to sharp structure in the XHX^- photoelectron spectrum with peak widths ultimately determined by the resonance lifetimes. The possibility of directly observing these states was a major motivating factor in our investigations. Although state-to-state reactive scattering experiments on the $F + H_2$ ²⁸ and $H + H_2$ ¹³ reactions show effects attributable to such resonances, the exact interpretation of these results is complicated by the large number of partial waves that contribute to the reaction cross section. This can result in direct scattering obscuring any effects due to resonances. Our experiment suppresses much of the contribution from direct scattering and restricts the total angular momentum available to the reaction, thereby enhancing the contribution from resonances. Aside from the interest in confirming the existence of these long-lived states, their observation would provide detailed information on the nature of the transition-state region for these reactions.

We have previously reported preliminary results on the $ClHCl^-$ photoelectron spectrum²⁹ taken with an earlier version of our photoelectron spectrometer. Although the resolution was poor (35 meV), the spectra showed resolvable structure which was attributed to the antisymmetric stretch of the $ClHCl$ collision complex. Since then the resolution of the instrument has been improved to $5\text{--}8 \text{ meV}$, and results on IHI^- were reported³⁰ that

(18) Bradforth, S. E.; Weaver, A.; Metz, R. B.; Neumark, D. M. *Advances in Laser Science—IV: Proceedings of the 1988 International Laser Science Conference*; American Institute of Physics Conference Proceedings 191; Gole, J. L., Heller, D. F., Lapp, M., Stwalley, W. C., Eds.; American Institute of Physics: New York, 1989; p 657.

(19) Kneba, M.; Wolfrum, J. *J. Phys. Chem.* **1979**, *83*, 69. Klein, F. S.; Persky, A.; Weston, R. E., Jr. *J. Chem. Phys.* **1964**, *41*, 1799.

(20) Garrett, B. C.; Truhlar, D. G.; Wagner, A. F.; Dunning, T. H., Jr. *J. Chem. Phys.* **1983**, *78*, 4400. Botschwina, P.; Meyer, W. *Chem. Phys. Lett.* **1976**, *44*, 449.

(21) Kawaguchi, K. *J. Chem. Phys.* **1988**, *88*, 4186.

(22) Botschwina, P.; Sebald, P.; Durmeister, R. *J. Chem. Phys.* **1988**, *88*, 5246; Ikuta, S.; Saitoh, T.; Nomura, O. *J. Chem. Phys.* **1989**, *91*, 3539.

(23) (a) Milligan, D. E.; Jacox, M. E. *J. Chem. Phys.* **1970**, *53*, 2034. (b) Nibler, J. W.; Pimentel, G. C., Jr. *J. Chem. Phys.* **1967**, *47*, 710. (c) Ault, B. J. *Acc. Chem. Res.* **1982**, *15*, 103.

(24) Truhlar, D. G.; Kuppermann, A. *J. Chem. Phys.* **1970**, *52*, 384. Wu, S.-F.; Levine, R. D. *Mol. Phys.* **1971**, *22*, 991.

(25) Bondi, D. K.; Connor, J. N. L.; Manz, J.; Römelt, J. *Mol. Phys.* **1983**, *50*, 467.

(26) Manz, J.; Meyer, R.; Schor, H. H. R. *J. Chem. Phys.* **1984**, *80*, 1562.

(27) Schatz, G. C. *Chem. Phys. Lett.* **1988**, *151*, 409.

(28) Neumark, D. M.; Wodtke, A. M.; Robinson, G. N.; Hayden, C. C.; Lee, Y. T. *J. Chem. Phys.* **1985**, *82*, 3045.

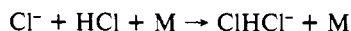
(29) Metz, R. B.; Kitsopoulos, T.; Weaver, A.; Neumark, D. M. *J. Chem. Phys.* **1988**, *88*, 1463.

strongly suggested the existence of long-lived (>0.1 ps) states of the IHI complex. Here we report the BrHBr^- and most recent ClHCl^- photoelectron spectra. The BrHBr^- spectrum is particularly amenable to detailed analysis, and we have used our spectrum to construct an "effective" collinear potential energy surface for the $\text{Br} + \text{HBr}$ reaction. The relationship between the potential energy surface and the experimental peak spacings, intensities, and widths is discussed, including the role of reactive resonance states and the possible contribution of transitions to electronically excited $\text{Br} + \text{HBr}$ potential energy surfaces.

Experimental Section

The negative ion time-of-flight photoelectron spectrometer³¹ used in these studies is shown in Figure 2. A gas mixture at a backing pressure of approximately 2 atm is expanded through a pulsed molecular beam valve (1) operating at 20 Hz. A 1-keV, 300- μA electron beam (2) crosses the gas jet just outside the nozzle, in the continuum flow region of the expansion. The fast electrons produce relatively low energy secondary electrons via ionization, and these secondary electrons rapidly thermalize due to the high gas density in this region. Negative ions formed through low-energy electron attachment processes should cool internally as the expansion progresses. We have measured a vibrational temperature of ≈ 150 K for CH_2CN^- in this source and a rotational temperature in the range of 50–75 K for SH^- produced in a similar source.³²

A mixture of 5% HBr in Ar was used to make BrHBr^- , presumably via dissociative electron attachment to HBr to form Br^- and subsequent clustering. In the ClHCl^- experiments, a mixture of 5% HCl seeded in He did not produce sufficient quantities of ions, probably due to the small cross section for dissociative attachment to HCl at low electron energy. Addition of CF_2Cl_2 resulted in a great improvement in ion signal. A mixture of 5% HCl and 25% CF_2Cl_2 seeded in He was used for the experiments. The likely mechanism for ClHCl^- formation is



The pressure in the source chamber, which is pumped with an Edwards 250M 10-in. diffusion pump, is typically 2×10^{-5} to 1×10^{-4} Torr.

The ions are mass selected with a Wiley-McLaren type time-of-flight mass spectrometer.³³ The ion source (including the pulsed valve, electron gun, and extraction plates) is floated at -1000 V with respect to ground. The ions are extracted (3) with a 10- μs , 100-V/cm pulse, through a 3-mm orifice into the first differential chamber, which is maintained at a pressure of 2×10^{-7} Torr by a 6-in. diffusion pump (Edwards 160M). The ions are then accelerated by 1 keV (to ground potential), pass through a second differentially pumped region, maintained at 2×10^{-8} Torr by a 150-L/s turbomolecular pump (Leybold-Heraeus), and enter the detection region. This region is also pumped by a 150-L/s turbomolecular pump and is maintained below 1.0×10^{-8} Torr. The ions are detected (5) 1.4 m from the extraction region, using a pair of 25-mm-diameter chevron-mounted microchannel plates (Galileo). Ion signal at the detector is maximized by using two sets of horizontal and vertical deflectors and an Einzel lens (4). The mass resolution of the spectrometer is 250–300. The ions studied in this work are $^{35}\text{ClH}^{35}\text{Cl}^-$ and $^{79}\text{BrH}^{79}\text{Br}^-$ and the deuterated species.

The mass-selected ions are detached (6) 10 cm in front of the ion detector by using a pulsed laser. A grid (7) in front of the

ion detector can be set at -1400 V to allow only neutrals created by photodetachment to pass. The laser firing delay is varied until optimal temporal overlap is achieved with the ion of interest, as monitored by observing the neutral signal with the grid voltage applied. The fifth harmonic (213 nm, 5.825 eV) of a Nd:YAG laser (Quanta-Ray DCR-3, 20-Hz rep rate) is used in the photodetachment studies reported here. This is generated by mixing the YAG laser fundamental with the fourth harmonic in a β -barium borate crystal (CSK Corporation). Typical pulse energies are 10–12 mJ. The laser beam is gently focused with a 200-cm lens to a 0.2-cm-diameter spot at the interaction region. The laser beam enters the machine through a MgF_2 window, passes through a series of light baffles, intersects the ion beam at right angles, passes through another set of light baffles, and exits through a quartz window.

The energy of the detached electrons is determined by time of flight. Photoelectrons are detected (8) at the end of a 1-m flight tube orthogonal to the laser and ion beams. The flight tube is magnetically shielded by two concentric cylinders (13- and 18-cm diameter) of Hypnom (9). The innermost surface of the shielding is coated with colloidal graphite (to eliminate patch potentials) and degaussed (to limit residual magnetic fields to 1–5 mG). Electrons are detected by a chevron-mounted pair of 40-mm-diameter microchannel plates. The signal is amplified and fed through a discriminator into a 200-MHz transient digitizer (LeCroy TR8828C), which is started by a photodiode triggered by a reflection from the laser. A signal averager (LeCroy 6010) reads the digitizer every laser shot, and the averager is read by an IBM AT computer every 250 shots. The entire timing sequence in the experiment is controlled by a Stanford Research Systems DG535 pulse generator. The electron detector subtends a solid angle of 0.0013 sr; 0.01% of the detached photoelectrons are detected.

Ultraviolet photons efficiently eject electrons from metal surfaces, so great care is taken to minimize background photoelectrons produced by stray photons striking metal surfaces in the detector region. The stray photons are largely eliminated by the light baffles between the interaction region and the entrance and exit windows. Additional discrimination against background photoelectrons is provided by four plates (10) (two round plates of 11-cm outer diameter with a 7.5-cm inner diameter hole, alternated with two 7.5-cm square plates with a 2-cm inner diameter hole) placed 5 cm apart, starting 28 cm up the flight tube. With these precautions, the residual background photoelectron contribution is 1 electron per laser shot at 213 nm. As the kinetic energy distribution of the background photoelectrons is smooth and does not change from day to day, a smooth function is fitted to the background, scaled, and subtracted from the spectrum.

Under typical conditions, the ion density in the laser interaction region ($\sim 0.01\text{-cm}^3$ volume) is about $10^5/\text{cm}^3$ for the ion of interest. At higher densities, the photoelectron spectrum shifts and broadens due to space charge. Between 10% and 50% of the ions are photodetached, and about 1 electron is detected per laser shot. A typical spectrum takes 300 000 laser shots. Photoelectron flight times (t) are converted to electron kinetic energy (eKE) by using

$$e\text{KE} = \frac{lm_e}{2(t - t_0)^2} \quad (1)$$

The time offset (t_0) and flight tube length (l) are determined by calibrating with F^- , Cl^- , Br^- , and I^- , all of which have known electron binding energies.

We have determined the resolution of the spectrometer to be

$$R \text{ (meV)} = \{25 + 180(e\text{KE})^3\}^{1/2} \quad (2)$$

where eKE is in electronvolts. The best resolution obtained is ≈ 5 meV at low energy, and the 11.5-ns combined time-width of the laser and electronics causes the resolution to degrade at higher electron energy.

Results and Preliminary Discussion

The 213-nm photoelectron spectra of ClHCl^- and ClDCl^- are shown in Figure 3. These spectra show partially resolved peaks

(30) Weaver, A.; Metz, R. B.; Bradforth, S. E.; Neumark, D. M. *J. Phys. Chem.* **1988**, *92*, 5558.

(31) Posey, L. A.; DeLuca, M. J.; Johnson, M. A. *Chem. Phys. Lett.* **1986**, *131*, 170. Cheshnovsky, O.; Yang, S. H.; Pettiette, C. L.; Craycraft, S. J.; Smalley, R. E. *Chem. Phys. Lett.* **1987**, *138*, 119. Gantefor, G.; Meiwes-Broer, K. H.; Lutz, H. O. *Phys. Rev. Lett.* **1988**, *37*, 2716.

(32) Kitsopoulos, T. N.; Waller, I. M.; Loeser, J. G.; Neumark, D. M. *Chem. Phys. Lett.* **1989**, *159*, 300.

(33) Wiley, W. C.; McLaren, I. H. *Rev. Sci. Instrum.* **1955**, *26*, 1150.

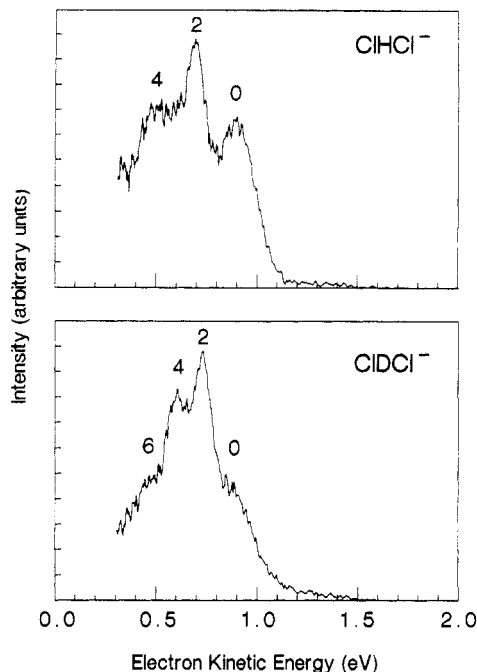


Figure 3. 213-nm photoelectron spectra of ClHCl⁻ and ClDCl⁻.

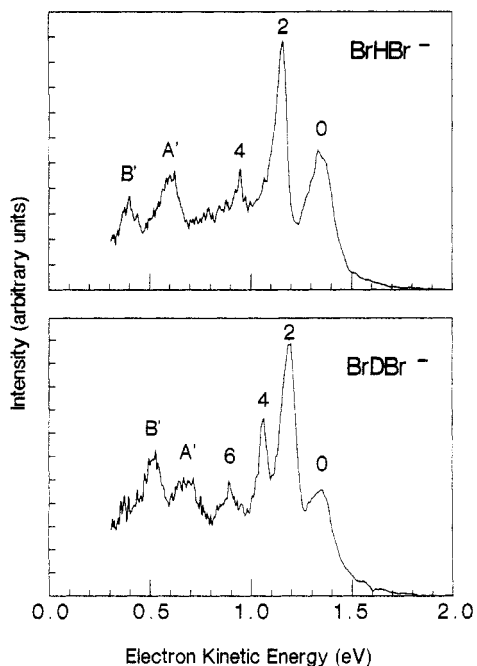


Figure 4. 213-nm photoelectron spectra of BrHBr⁻ and BrDBr⁻.

and are similar to the spectra reported earlier²⁹ at considerably lower (35 meV) resolution. In contrast, the 213-nm photoelectron spectra of BrHBr⁻ and BrDBr⁻ (Figure 4) show a series of well resolved peaks with widely varying widths. The peak positions and widths are given in Table I. The positions of the highest energy peaks in the ClHCl⁻ and BrHBr⁻ spectra are unchanged by deuteration, whereas the remaining peaks shift to higher electron energy. The peak spacings and intensities for the ClHCl⁻ and ClDCl⁻ spectra are the same as those previously observed at 193 nm. This shows the spectra result from direct photodetachment to the (neutral + e⁻) continuum rather than autodeachment from an excited electronic state of the ion.

We now consider some general features of these results. The first question is whether the peaks in these spectra correspond to transitions to levels of the neutral XHX complex that are bound or unbound with respect to X + HX ($v = 0$). This can be determined with the aid of Figure 5, which is drawn for the BrHBr⁻ system. This figure shows that peaks with electron kinetic energy

TABLE I: Peak Positions and Widths in the 213-nm (5.825 eV) Photoelectron Spectra of ClHCl⁻ and ClDCl⁻ and of BrHBr⁻ and BrDBr⁻

v_3'	eKE, eV	width, meV	
ClHCl ⁻			
0	0.894	130	
2	0.693	85	
4	0.517	- ^c	
ClDCl ⁻			
0	0.884	- ^c	
2	0.734	70	
4	0.611	55	
6	0.479	- ^c	
v_3'	eKE, eV	width, meV	asympt, eV
BrHBr ⁻			
0	1.353	170	1.554
2	1.159	80	1.237
4	0.950	20	0.931
A'	0.608	140	
B'	0.397	140	
BrDBr ⁻			
0	1.344	175	1.560
2	1.190	100	1.332
4	1.061	64	1.109
6	0.895	20	0.892
A'	0.686	140	
B'	0.529	140	

^a Average uncertainty in peak positions is 0.015 eV. ^b The asymptotes correspond to Br + H(D)Br ($v = v_3'/2$). Average uncertainty in peak positions is 0.010 eV. ^c Accurate widths could not be determined, as these peaks were not sufficiently well resolved.

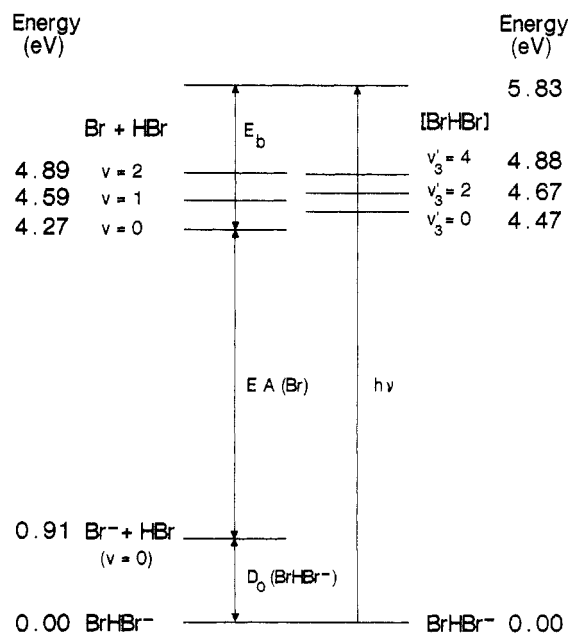


Figure 5. Energy level diagram for the BrHBr⁻/[BrHBr] system. The uncertainty in $D_0(\text{BrHBr}^-)$ is 0.05 eV.

less than $E_b = h\nu - D_0(\text{BrHBr}^-) - \text{EA}(\text{Br})$ result from levels of the neutral complex that lie above Br + HBr ($v = 0$). Here, $h\nu$ is the photon energy (5.825 eV), $D_0(\text{BrHBr}^-)$ is the energy needed for the dissociation reaction $\text{BrHBr}^- \rightarrow \text{Br}^- + \text{HBr}$, and $\text{EA}(\text{Br})$ is the electron affinity of Br. $D_0(\text{BrHBr}^-)$ has been determined by high-pressure mass spectroscopy to be 0.91 ± 0.05 eV,³⁴ and with $\text{EA}(\text{Br}) = 3.365$ eV,³⁵ we find $E_b = 1.55 \pm 0.05$ eV. For ClHCl⁻, $D_0(\text{ClHCl}^-) = 1.02 \pm 0.05$ eV,³⁴ $\text{EA}(\text{Cl}) = 3.617$ eV,³⁵ and $E_b = 1.19 \pm 0.05$ eV. The peak at highest electron kinetic energy appears at 1.353 eV for BrHBr⁻ and 0.894 eV for ClHCl⁻,

(34) Caldwell, G.; Kebarle, P. *Can. J. Chem.* **1985**, *63*, 1399.

(35) Hotop, H.; Lineberger, W. C. *J. Phys. Chem. Ref. Data* **1985**, *14*, 731.

so *all* the observed peaks for both systems result from transitions to unbound states of the neutral complex. This suggests that the potential energy surfaces for the Cl + HCl and Br + HBr reactions have barriers but no wells near the transition state. Although there has been considerable discussion of "vibrationally bound states"³⁶ of IHI and (less so) for BrHBr, this would require peaks with electron kinetic energy above E_b . Our results here and those presented earlier³⁰ for IHI⁻ show no evidence for this.

We next consider the isotope effects observed in the spectra. The peak shifts show we are observing a vibrational progression in a mode involving H atom motion, and one must determine if this is a progression in the ion ("hot band" transitions) or the neutral. As long as the active vibrational mode is not the dissociation coordinate of the complex (see next section), the electron kinetic energy from a neutral \leftarrow ion transition is given by

$$E = h\nu - [D_0(\text{XHX}^-) + EA(\text{X}) + \Delta E] - E_{v''}^{(0)} + E_{v'}^{(0)} \quad (3)$$

Here ΔE is the vibrational zero point and electronic energy of the XHX complex relative to X + HX ($v = 0$). In Figure 5, for example, $\Delta E = 4.47 - 4.27 = 0.20$ eV. $E_{v''}^{(0)}$ and $E_{v'}^{(0)}$ are the rotational and vibrational energy in the active mode for the ion and neutral, respectively. Assuming similar zero-point energies for the ion and neutral, eq 3 predicts that the ($v' = 0$) \leftarrow ($v'' = 0$) transition should not shift upon deuteration, ($v' > 0$) \leftarrow ($v'' = 0$) transitions to excited vibrational levels of the neutral should shift to *higher* electron kinetic energies, and "hot band" ($v' = 0$) \leftarrow ($v'' > 0$) transitions should shift to *lower* electron energies. Here v'' and v' are vibrational quantum numbers for the active mode in the ion and neutral, respectively. The highest energy peak in the experimental spectrum does not shift upon deuteration, so this peak is the $0 \leftarrow 0$ transition, and the spectra represent a ($v' = n$) \leftarrow ($v'' = 0$) progression in a vibrational mode of the *neutral complex*. None of the peaks appear to arise from hot bands.

The active mode could be either the bend (v_2) or antisymmetric stretch (v_3) of the complex. Since the ions are linear and the minimum energy paths for the reactions are likely to be nearly collinear,²⁰ an extended progression in the bend is unlikely, and we assign the peaks to a progression in the v_3 mode. Symmetry considerations show that only transitions to even v_3' levels of the complex are allowed from the $v_3'' = 0$ level of the ion.³⁷ The peaks in each spectrum are labeled by their v_3' quantum number in Table I. As discussed in more detail below, the two broad peaks at lowest energy in the BrHBr⁻ and BrDBr⁻ spectra (*A'* and *B'*) do not appear to belong to the same progression as that of the higher energy peaks.

The energies of the v_3' states for the BrHBr complex and the Br + HBr asymptotic vibrational energy levels are shown in Figure 5. The vibrational spacing in the BrHBr complex is significantly smaller than that in free HBr. The intuitive explanation for this is that the strong HBr bond in free HBr is replaced by two much weaker bonds in the BrHBr complex. This observation is therefore a strong indication that we are probing the transition-state region of the potential energy surface, where the hydrogen is interacting strongly with both bromine atoms.

Analysis and Discussion

The analysis of the vibrational structure in these spectra centers on the calculation of Franck-Condon factors for transitions between the ion and the neutral potential energy surface. The goal is to (a) understand the origin of the observed structure in the spectra and (b) use our results to learn about the transition-state region of the potential energy surfaces for the Cl + HCl and Br + HBr reactions. The ClHCl⁻/Cl + HCl system is the better characterized of the two. Several potential energy surfaces have been proposed for the Cl + HCl reaction,^{20,25,38} the ion geometry

TABLE II: Anion Frequencies (in cm^{-1})

	ClHCl ⁻		ClDCl ⁻ matrix	BrHBr ⁻ matrix	BrDBr ⁻ matrix
	gas ^a	matrix ^b			
ν_1''	318	260	267	164	170
ν_2''	792				
ν_3''	722.9	696	463	728	498

^aReference 21. ^bReference 42.

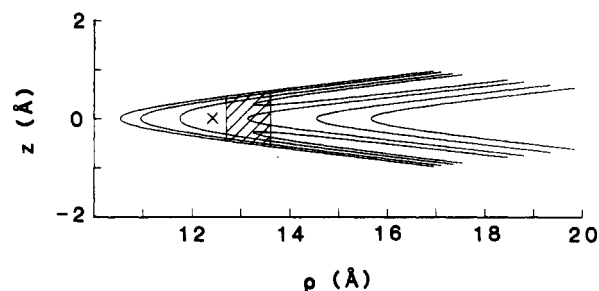


Figure 6. Contour plot of the BCMR LEPS potential for the collinear Cl + HCl system. The hyperspherical coordinates $z \approx 1/2(R_{\text{ClH}} - R_{\text{HCl}})$ and $\rho \approx 4.22R_{\text{Cl-Cl}}$ are used (eq 4). Contours are at -300, -350, -400, and -425 kJ/mol, with respect to three-atom dissociation. The Franck-Condon region is shaded.

has been experimentally determined,²¹ and simulations of the ClHCl⁻ photoelectron spectrum have been calculated, using some of the model surfaces for the reaction.^{39,40} These results will be used to explain the qualitative features of our spectra and to test the validity of the approximations used in our analysis. However, the peaks in the BrHBr⁻ spectra are better resolved, so we are able to extract considerably more information on the Br + HBr reaction.

Our analysis requires knowledge of the geometry and potential functions for the XHX⁻ ions. The ClHCl⁻ results discussed in the Introduction indicate that the ion is linear and centrosymmetric with an interhalogen distance R_e of 3.1122 Å.²¹ A MRD-CI calculation⁴¹ on BrHBr⁻ yields a linear, centrosymmetric structure with $R_e = 3.43$ Å. We assumed $R_e = 3.50$ Å in our analysis; this is within the error of the calculation and greatly facilitated fitting our results with a reasonable potential energy surface (see below).

The potential functions for the ions are inferred from the measured vibrational frequencies. Table II lists the gas-phase frequencies²¹ for the three vibrational modes of ClHCl⁻ and matrix isolation values for the symmetric (ν_1) and antisymmetric (ν_3) stretch frequencies in ClHCl⁻, ClDCl⁻, BrHBr⁻, and BrDBr⁻.⁴² The similarity between the gas-phase and matrix frequencies for ClHCl⁻ (and for FHF⁻⁴³) suggests that the matrix values for BrHBr⁻ and BrDBr⁻ can be used in our analysis, since the gas-phase values are unknown. For both ClHCl⁻ and BrHBr⁻, the matrix results for the antisymmetric stretch yield $\nu_{\text{H}}/\nu_{\text{D}} > 1.40$, the value expected for a harmonic oscillator. This "negative anharmonicity" implies that the potential function for the ν_3 mode is approximately harmonic with a small quartic contribution.^{23c} In our analysis, all the transitions in the spectra are assumed to originate from the ground vibrational state of the ion for which anharmonic effects should be small. We therefore neglected the quartic term and used harmonic oscillator wave functions with the frequencies given in Table II for the vibrational modes in all the ions.

As a first step in analyzing our results, consider the collinear London-Eyring-Polanyi-Sato (LEPS) potential energy surface⁴⁴ for the reaction $\text{Cl} + \text{HCl} \rightarrow \text{HCl} + \text{Cl}$ shown in Figure 6. This surface, which has a barrier of 36 kJ/mol, was constructed by

(36) Pollak, E. *J. Chem. Phys.* **1983**, *78*, 1228. Manz, J.; Meyer, R.; Pollak, E.; Römelt, J.; Schor, H. H. *R. Chem. Phys.* **1984**, *83*, 333. Clary, D. C.; Connor, J. N. L. *J. Phys. Chem.* **1984**, *88*, 2758.

(37) Herzberg, G. *Molecular Spectra and Molecular Structure, Vol. III*; Van Nostrand: New York, 1966; pp 150-157.

(38) (a) Persky, A.; Kornweitz, H. *J. Phys. Chem.* **1987**, *91*, 5496. (b) Last, I.; Baer, M. *J. Chem. Phys.* **1983**, *80*, 3246.

(39) Schatz, G. C. *J. Chem. Phys.* **1989**, *90*, 3582.

(40) (a) Bowman, J. M.; Gazdy, B. *J. Phys. Chem.* **1989**, *93*, 5129. (b) Gazdy, B.; Bowman, J. M. *J. Chem. Phys.* **1989**, *91*, 4615.

(41) Sannigrahi, A. B.; Peyerimhoff, S. D. *J. Mol. Struct.* **1988**, *165*, 55.

(42) Jacox, M. E. *J. Phys. Chem. Ref. Data* **1984**, *13*, 945.

(43) Kawaguchi, K.; Hirota, E. *J. Chem. Phys.* **1987**, *87*, 6838.

(44) Sato, S. *Bull. Chem. Soc. Jpn.* **1955**, *28*, 450.

Bondi et al.²⁵ on the basis of rate constant measurements by Kneba and Wolfrum.¹⁹ The surface (henceforth referred to as the BCMR LEPS) is plotted by using modified hyperspherical coordinates ρ and z ,⁴⁵ which, for the heavy plus light-heavy mass combination, simplify to

$$\rho \approx (m_{\text{Cl}}/2m_{\text{H}} + 1/2)^{1/2}R_{\text{Cl-Cl}} = 4.22R_{\text{Cl-Cl}} \quad (4a)$$

$$z \approx \frac{1}{2}(R_{\text{ClH}} - R_{\text{HCl}}) \quad (4b)$$

ρ and z represent the size and asymmetry, respectively, of the Cl + HCl system. The coordinate ρ is proportional to the symmetric stretch symmetry coordinate in ClHCl⁻, and $z \approx Q_3/2^{1/2}$, where Q_3 is the antisymmetric stretch symmetry coordinate. The skew angle in the figure is given by

$$\phi_{\text{max}} = \tan^{-1} \{ [m_{\text{H}}(m_{\text{H}} + 2m_{\text{Cl}})/m_{\text{Cl}}^2]^{1/2} \} = 13.6^\circ \quad (5)$$

where $m_{\text{H}} = 1.008$ amu and $m_{\text{Cl}} = 34.969$ amu.

The shaded region in Figure 6 indicates the area on the neutral surface that is directly probed by our photodetachment experiment. The center of the shaded region, at $z = 0$, $\rho = 13.15$ Å, corresponds to R_c for the ion. The extent of the shaded region represents the zero-point amplitude for the symmetric stretch in the ground vibrational state of the ion. Our spectra are very sensitive to the details of this "Franck-Condon region" of the potential energy surface.

Figure 6 shows that the Franck-Condon region does not include the saddle point, which is not a serious limitation. Calculations by Bondi et al.^{46a} and Hartke and Manz^{46b} indicate that relatively few reactive trajectories actually cross the saddle point because of the acute skew angle for a heavy plus light-heavy reaction such as Cl + HCl. At energies below the barrier height, the reaction rate is dominated by tunneling through the ridge that bisects the shaded region in the figure. At energies above the barrier height, most reactive trajectories cross from the reactant to product valley before reaching the saddle point. Thus, our experiment probes the "chemically relevant" part of this potential energy surface.

Figure 6 illustrates why a progression in the antisymmetric stretch is observed, even though the complex can dissociate. Near the center of the shaded region, motion along the z coordinate corresponds to the antisymmetric stretch of the neutral complex. This motion is nearly perpendicular to the minimum energy path which leads to dissociation via the reactant or product valleys. The antisymmetric stretch of the complex is therefore poorly coupled to the reaction coordinate in the region of the potential energy surface probed by our experiment. This is another consequence of the small skew angle for the collinear surface. Even though photodetachment of ClHCl⁻ produces a complex that dissociates, we observe a progression in a vibrational mode not strongly coupled to the dissociation coordinate. Similar effects have been proposed to explain vibrational structure in electronic absorption to dissociative states of neutral molecules.⁴⁷

The discussion so far suggests that we should be able to explain the experimental peak positions and intensities with a one-dimensional model in which only the antisymmetric stretch of the complex is considered. This is discussed in more detail in the following section.

1. One-Dimensional Approach. As discussed above, the peaks in the spectra originate from the $v_3'' = 0$ level of the anion, and this is assumed to be described by a harmonic oscillator wave function. For the LEPS surface in Figure 6, one can obtain an approximate potential function for the v_3' mode in the neutral complex by taking a cut at constant ρ through the center of the shaded region. The resulting double minimum potential is shown

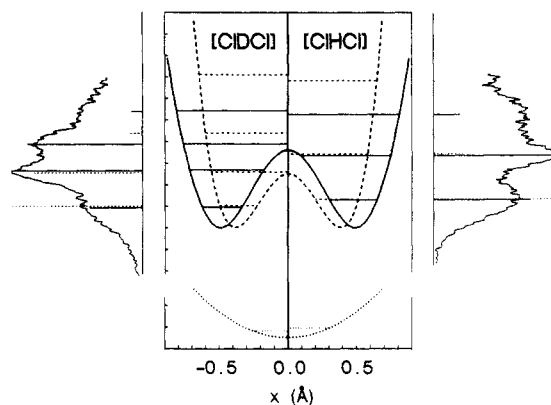


Figure 7. (bottom, ...) Harmonic potential for v_3 mode of ClHCl⁻ with $v_3'' = 0$ levels for ClHCl⁻ (right) and ClDCl⁻ (left). The abscissa $x = 2^{1/2}z$. (top and sides) Antisymmetric stretch potential for [ClHCl] from a cut through the BCMR LEPS potential at $R_{\text{Cl-Cl}} = 3.112$ Å (---) and double minimum potential which give best fit to experiment (—). For each potential, eigenvalues with even v_3' are shown, as are the "stick" spectra obtained from one-dimensional simulations of ClHCl⁻ and ClDCl⁻ photoelectron spectra. (The odd eigenfunctions have zero overlap with the ground state of the ion.) The simulations are superimposed on the experimental spectra. Each tick mark on the vertical axis is 0.1 eV. The parameters for the best fit double minimum potential are given in Table III.

in Figure 7 (dashed line), above the harmonic oscillator potential assumed for the ion (dotted line). The neutral \leftarrow ion transition involves going from a single to a double minimum potential for the antisymmetric stretch; this is why the v_3' mode is active in our spectra.

We numerically solve for the eigenvalues and eigenfunctions supported by this potential. A simulated "one-dimensional" photoelectron spectrum is obtained by calculating the Franck-Condon overlap between the $v_3'' = 0$ wave function of the ion and the v_3' wave functions supported by the double minimum potential.⁴⁸ This overlap is zero for all odd v_3' . The simulated ClHCl⁻ and ClDCl⁻ spectra from the LEPS surface are shown in Figure 7 superimposed on the experimental spectra. The peak spacings and intensities in the stick spectra show some resemblance to the broad peaks in the experimental spectra. In particular, the higher $v_3' = 0/v_3' = 2$ ratio in the experimental ClHCl⁻ spectrum relative to the ClDCl⁻ spectrum appears in the simulation. This is a consequence of the lower energy $v_3' = 0$ wave function for the ClDCl complex having less probability near $z = 0$ and hence poorer overlap with the $v_3'' = 0$ wave function for the ion.

However, the peak spacing in the simulated spectra is too large, and the overall intensity distribution is incorrect. As a first step toward determining the true potential energy surfaces for the Cl + HCl and Br + HBr reactions, we have constructed empirical double minimum potentials with adjustable parameters to better reproduce the experimental results for these systems. These are functions of the antisymmetric stretch symmetry coordinate $Q_3 = x = (R_{\text{Cl-H}} - R_{\text{H-Cl}})/2^{1/2}$:

$$V(x) = b + \frac{1}{2}k(x - x_1)^2 + q(x - x_1)^4 \quad \text{for } x > x_1 \quad (6a)$$

and

$$V(x) = b + h - d(x - x_1)^2 + e(x - x_1)^4 + f(x - x_1)^6 \quad \text{for } x \leq x_1 \quad (6b)$$

Equations 6a and 6b are for $x \geq 0$. For $x < 0$, $V(x) = V(-x)$. The complete potential function has two minima at $x = \pm x_1$ separated by a barrier of height h at $x = 0$. The parameters k and q determine the steepness of the outer walls. The other (dependent) parameters are given by $d = k/8 + ex_1^2$, $e = 3h/x_1^4 - k/4x_1^2$, and $f = (k - 8ex_1^2)/24x_1^2$. These conditions ensure that the potential and its first and second derivatives are continuous.

(48) We thank G. Barney Ellison for a copy of his program for calculating Franck-Condon factors.

(45) Hauke, G.; Manz, J.; Römelt, J. *J. Chem. Phys.* **1980**, *73*, 5040. Kuppermann, A.; Kaye, J. A.; Dwyer, J. P. *Chem. Phys. Lett.* **1980**, *74*, 257. Babamov, V. K.; Marcus, R. A. *J. Chem. Phys.* **1981**, *74*, 1790. Aquilanti, V.; Cavalli, S.; Lagana, A. *Chem. Phys. Lett.* **1982**, *93*, 179.

(46) (a) Bondi, D. K.; Connor, J. N. L.; Garrett, B. C.; Truhlar, D. G. *J. Chem. Phys.* **1983**, *78*, 5981. (b) Hartke, B.; Manz, J. *J. Am. Chem. Soc.* **1988**, *110*, 3063.

(47) Pack, R. T. *J. Chem. Phys.* **1976**, *65*, 4765.

TABLE III: Potential Parameters for the One-Dimensional Fits^a

	[ClHCl]	[BrHBr]	[BrHBr]*
x_1 , Å	0.49	0.45	0.47
h , kJ/mol	35	30	52
k , (kJ/mol)/Å ²	1000	500	450
q , (kJ/mol)/Å ⁴	0	2500	2500

^aThe form of the potential is eq 6.

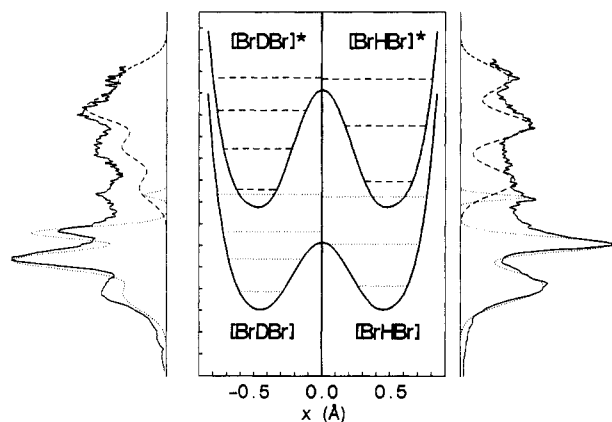


Figure 8. Best fit antisymmetric stretch potentials for [BrHBr] and [BrHBr]* and resulting spectra. Energy levels for even v_3' states supported by each potential are shown (... for [BrHBr], --- for [BrHBr]*), as are results of one-dimensional simulation of BrHBr⁻ and BrDBr⁻ photoelectron spectra. For comparison with experiment, the Franck-Condon sticks have been convoluted with Gaussians to match the experimental peak widths. Each tick mark on the vertical axis is 0.1 eV. The parameters for the potentials are given in Table III.

The potential of this form that best fits the ClHCl⁻ and ClDCI⁻ results is drawn with a solid line in Figure 7, superimposed on the double minimum potential derived from the LEPS surface. The one-dimensional simulations obtained from this potential are also shown in Figure 7. The parameters for the optimal double minimum potential are given in Table III. Although the barrier is slightly higher in our potential, the biggest difference is that the outer walls are too steep and the separation between the minima is too small in the LEPS potential. The simulated peak spacings from a LEPS surface therefore tend to be too large, and the simulated $v_3' = 0$ peak is too intense. These discrepancies with experiment were also seen in the IHI⁻/I + HI system when the spectrum was simulated with a LEPS surface.³⁰

The positions and intensities of the three highest energy peaks in the BrHBr⁻ spectrum and the first four peaks in the BrDBr⁻ spectrum were simulated by using the double minimum potential in the lower half of Figure 8. The simulated spectrum from this potential is shown with dotted lines in Figure 8. Because of the large variation in the experimental peak widths, the width of each simulated peak is set equal to the experimental width to facilitate comparison with the experimental intensities. The area under each simulated peak would give the relative height in a simulated stick spectrum.

The two broad low-energy peaks (*A'* and *B'*) present more of a problem. These peaks do not seem to belong to the same vibrational progression as the higher energy peaks. It is not clear how a bimodal intensity distribution could arise if all the peaks were due to the same progression. In addition, the spacing between the $v_3' = 4$ peak and peak *A'* in the BrHBr⁻ spectrum is nearly 0.35 eV, an anomalously large value that is greater than the HBr fundamental frequency. A possible explanation is that peaks *A'* and *B'* are part of a second vibrational progression arising from a low-lying excited electronic state of the complex. The large isotope shift of peak *A'* indicates that it is not the origin of this progression. However, adding the *A'*-*B'* splitting to the energy of peak *A'* gives a value of 0.82 eV in the BrHBr⁻ spectrum and 0.84 eV in the BrDBr⁻ spectrum. This suggests that peaks *A'* and *B'* are the second and third peaks in a vibrational progression for which the origin is not observed.

The entire spectrum for each isotope can be simulated by assuming peaks *A'* and *B'* result from transitions to the $v_3' = 2$ and $v_3' = 4$ levels of the upper double minimum potential shown in Figure 8. The simulated spectrum from this potential is indicated with a dashed line in Figure 8. The high barrier between the wells makes the $0 \leftarrow 0$ transition very weak. Note that the simulation suggests that the broad feature under the narrow $v_3' = 6$ peak in the BrDBr⁻ spectrum is the $0 \leftarrow 0$ transition in the second progression.

The $v_3' = 0$ peaks of the two progressions in Figure 8 are separated by 0.49 eV. This is slightly larger than the $^2P_{1/2}$ - $^2P_{3/2}$ spin-orbit splitting in the Br atom (0.45 eV) and suggests that the second progression is due to an electronically excited state of the complex that asymptotically correlates to Br*($^2P_{1/2}$) + HBr. Based on diatomics-in-molecules (DIM) calculations⁴⁹ on F + HF and Cl + HCl, this excited-state interaction is expected to be considerably more repulsive than the ground state. The high barrier between the wells in Figure 8 is consistent with a repulsive interaction. We have observed other examples of transitions to spin-orbit excited surfaces in IHI⁻ and several asymmetric bihalides¹⁸ which will be reported in detail in the near future. Based on these considerations, it is quite possible that the ClHCl⁻ and ClDCI⁻ photoelectron spectra also contain transitions to electronically excited states of the neutral complex. These transitions could give rise to broad peaks that interfere with the ground-state spectra.

The one-dimensional analysis outlined here provides a useful first-order explanation of our experimental results. The reasonable agreement between experimental and simulated peak spacings and intensities supports the assignment of the structure in our spectra to a progression in the antisymmetric stretch of the complex. However, this analysis does not explain the dramatic variation in the peak widths observed in the BrHBr⁻ and BrDBr⁻ spectra. The peak widths are sensitive to the dynamics of the complex along the reaction coordinate. The analysis of the peak widths requires a more sophisticated, two-dimensional method that is discussed in detail in the next section.

2. Two-Dimensional Analysis. A rigorous simulation of our results requires calculation of the Franck-Condon overlap between the bound ionic vibrational states and the full scattering wave functions supported by the three-dimensional reactive potential energy surface. Schatz³⁹ has recently simulated parts of the ClHCl⁻ and IHI⁻ photoelectron spectra by using three-dimensional scattering wave functions with the restriction that the ion is in its ground vibrational state and that total angular momentum $J = 0$ for the ion and the final scattering states. Even with these restrictions on the ion and total angular momentum, the calculations are quite involved and have only been performed on model LEPS surfaces for the Cl + HCl and I + HI reactions. Gazdy and Bowman^{40b} have also calculated three-dimensional ($J = 0$) simulations of these photoelectron spectra, using an L^2 basis set.

Our goal is to use the experimental results to construct better potential energy surfaces for these reactions. We use an iterative approach, since the experimental results cannot be directly inverted to give the potential energy surface. A flexible functional form is chosen for the potential energy surface, and the parameters are adjusted until simulations reproduce experimental results. This procedure would be far too time-consuming if a full three-dimensional simulation were performed for each iteration. We have therefore used an approximate scheme that is essentially a two-dimensional simulation. The aim here is to use our calculation to devise a surface that reproduces the experimental spectra. Once this is determined, a more sophisticated simulation could be performed to check the accuracy of the resulting potential energy surface.

Our simulations incorporate two significant approximations concerning the scattering wave function on the neutral surface. First, the three-dimensional potential energy function $V(\rho, z, \gamma)$ (where ρ and z were defined previously and γ is the X-H-X

(49) Firth, N. C.; Grice, R. J. *Chem. Soc., Faraday Trans. 2* **1987**, *87*, 1023.

bending angle) is reduced to an "effective" collinear potential energy surface $V(\rho, z)$ via

$$V(\rho, z) = V(\rho, z, \gamma = \pi) + \epsilon_0(\rho, z) \quad (7)$$

Here $\epsilon_0(\rho, z)$ is the bending zero-point energy for the linear configuration of the nuclei specified by ρ and z . Equation 7 results from the adiabatic bend theory developed by Bowman⁵⁰ as part of his reduced dimensionality model of reactive scattering. This assumes that the bending mode is separable from the other degrees of freedom of the system. Equation 7 includes the change in bending zero-point energy with the size and asymmetry of the complex and therefore incorporates some effects of the bending mode into our analysis. From the point of view of our experiment, we are assuming that only transitions to the lowest bending level of the neutral complex occur. This theory should be reasonably accurate if the reaction is collinearly dominated, so that photo-detachment of a linear ion should not produce substantial bending excitation in the neutral complex. One can also construct effective collinear surfaces for bend-excited states ($v_2' = n$) of the complex by substituting $\epsilon_n(\rho, z)$ for $\epsilon_0(\rho, z)$ in eq 7.

We now have to find the scattering wave function $\psi(\rho, z)$ supported by the effective collinear potential $V(\rho, z)$. In these coordinates, the Schrodinger equation is

$$-\frac{1}{2m} \left[\frac{\partial^2}{\partial \rho^2} + \frac{1}{\rho} \frac{\partial}{\partial \rho} + \frac{\partial^2}{\partial z^2} + V(\rho, z) \right] \psi(\rho, z) = E \psi(\rho, z) \quad (8)$$

where m is the reduced mass of HX. We now invoke our second approximation, an adiabatic approximation that has been used by several investigators^{25,36,45} in studies of collinear heavy plus light-heavy reactions. We assume the scattering wave function can be written as a product of two wave functions:

$$\psi(\rho, z) = \theta_{v_3}(z; \rho) R_{v_3}(\rho) \quad (9)$$

This is analogous to the Born-Oppenheimer approximation in diatomic molecules. $\theta_{v_3}(z; \rho)$ is the wave function for the fast antisymmetric stretch vibration along the z direction and depends weakly on ρ . $R_{v_3}(\rho)$ is either a symmetric stretch or translational wave function that primarily involves relatively slow heavy-atom motion. θ_{v_3} and R_{v_3} satisfy the one-dimensional equations

$$\left[-\frac{1}{2m} \frac{\partial^2}{\partial z^2} + V(\rho, z) \right] \theta_{v_3}(z; \rho) = \epsilon_{v_3}(\rho) \theta_{v_3}(z; \rho) \quad (10a)$$

and

$$\left[-\frac{1}{2m} \frac{\partial^2}{\partial \rho^2} + U_{v_3}(\rho) \right] R_{v_3}(\rho) = E R_{v_3}(\rho) \quad (10b)$$

where

$$U_{v_3}(\rho) = \epsilon_{v_3}(\rho) - \frac{1}{8m\rho^2} - \frac{1}{2m} Q_{v_3 v_3} \quad (11)$$

Equation 10a is essentially the same one-dimensional Schrodinger equation that was solved in the last section to obtain the antisymmetric stretch eigenvalues and eigenfunctions for the neutral complex. By solving eq 10a at many values of ρ , one generates a set of curves $\epsilon_{v_3}(\rho)$ that map out the energy of the v_3 antisymmetric stretch level as a function of the size of the complex and a set of antisymmetric stretch eigenfunctions $\theta_{v_3}(z; \rho)$ that depend parametrically on ρ . For a symmetric X + HX system, one finds two adiabatic curves that correlate to each X + HX ($v = m$) asymptotic state; these curves have $v_3 = 2m$ and $v_3 = 2m + 1$ and correspond to wave functions θ_{2m} and θ_{2m+1} , which are of even and odd parity, respectively.

Equation 10b for $R_{v_3}(\rho)$ is a one-dimensional Schrodinger equation for a particle with total energy E moving in an effective or adiabatic potential $U_{v_3}(\rho)$. The adiabatic potential is determined by the solutions to (10a) according to (11). The DIVAH cor-

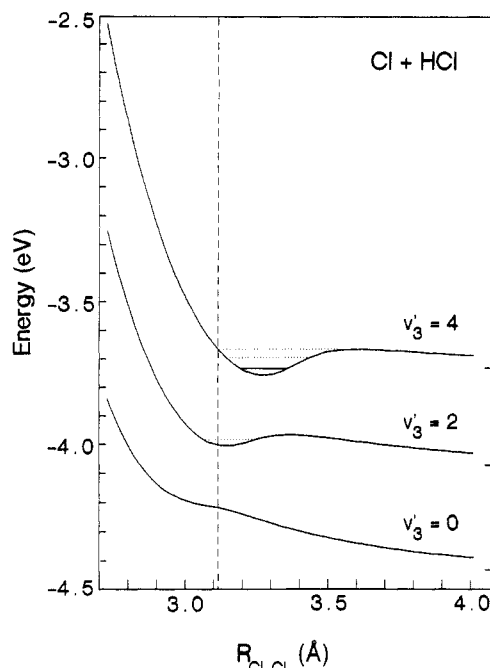


Figure 9. Adiabatic curves $U_{v_3}(\rho)$ for Cl + HCl on the BCMR LEPS potential (ref 25), including zero-point bend. Shape resonances are denoted by dotted lines, and the Feshbach resonance is shown by a solid line. The asymptotic energy levels of Cl + HCl ($v = v_3/2$) are denoted by arrows. The dashed line is drawn at R_e for ClHCl⁻ ($R_{\text{Cl-Cl}} = 3.112$ Å; $\rho = 13.15$ Å).

rection⁵¹ $Q_{v_3 v_3}$ (eq 11) is very small for a heavy plus light-heavy reaction.

Figure 9 shows the first few adiabatic curves for the Cl + HCl reaction, obtained from the effective collinear surface derived from the three-dimensional BCMR LEPS surface.²⁵ These curves are similar to those in ref 25, but they also include the bending zero-point energy. For a purely repulsive adiabatic potential such as $U_0(\rho)$ in Figure 9, the solutions $R_0(\rho)$ are one-dimensional continuum scattering wave functions. The $U_2(\rho)$ and $U_4(\rho)$ potentials each have a well, separated by a barrier from the Cl + HCl($v=1$) and Cl + HCl($v=2$) asymptotes, respectively. In addition to supporting continuum states, these potentials support long-lived *symmetric stretch* levels, which lead to the sharp resonance structure seen in collinear reactive scattering calculations on this surface. The U_2 potential supports a narrow "shape resonance", indicated with a dotted line in Figure 9. This is a long-lived state of the complex that can decay either by tunneling through the barrier on the U_2 potential to Cl + HCl($v=1$) or by undergoing vibrational predissociation to form Cl + HCl($v=0$). The U_4 potential supports several shape resonances as well as a state (indicated with a solid line) that lies below the Cl + HCl($v=2$) asymptote. This is a "Feshbach resonance", which can decay only by vibrational predissociation.

In our adiabatic approximation, coupling between the potentials $U_{v_3}(\rho)$ is neglected and vibrational predissociation is not allowed. Thus, Feshbach resonances cannot decay, and shape resonances can decay only by tunneling. Since collinear and three-dimensional scattering calculations show that these resonances are narrower than our experimental resolution, we treat both types of resonances as bound states with widths determined by the experimental resolution. The resonance wave functions are assigned a symmetric stretch quantum number v_1 based on the number of nodes inside the well in the adiabatic potential.

The adiabatic potentials are instrumental in simulating the negative ion photoelectron spectrum. We calculate the Franck-Condon overlap between the initial state of the ion and the bound and continuum states supported by the adiabatic potentials $U_{v_3}(\rho)$. The intensity of a transition from an ion in its (v_1'', v_3'') vibrational

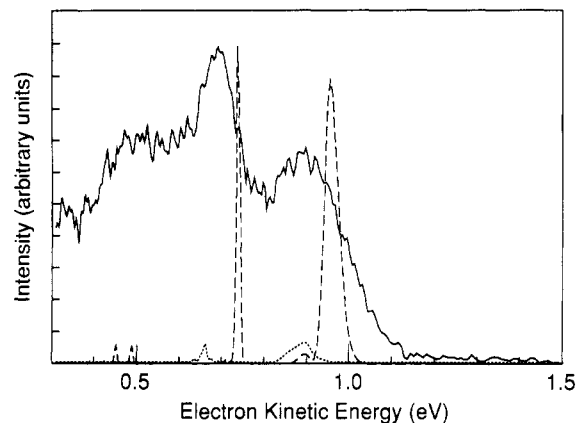


Figure 10. Two-dimensional simulated photoelectron spectrum of ClHCl⁻ using the BCMR LEPS potential including zero-point bend superimposed on experimental spectrum for different bending levels of [ClHCl] (---, $v_2' = 0$; ..., $v_2' = 2$). The simulated spectrum has been convoluted with the experimental resolution (eq 2) and assumes the ion is in its ground vibrational state.

level to a resonance state with symmetric stretch wave function $R_{v_1',v_3'}(\rho)$ and antisymmetric wave function $\theta_{v_3'}(z;\rho)$ is proportional to

$$\int d\rho \left\{ \int dz \theta_{v_3'}(z;\rho) \psi_{-v_3'}^-(z) \right\} R_{v_1',v_3'}(\rho) \psi_{-v_1'}^-|^2 \quad (12)$$

where $\psi_{-v_1'}^-$ and $\psi_{-v_3'}^-(z)$ are harmonic oscillator wave functions for the symmetric and antisymmetric stretch, respectively, in the ion. Such a transition yields a sharp peak in the simulated spectrum. A broad peak can arise from transitions to continuum states supported by an adiabatic potential. For example, transitions to the repulsive $U_0(\rho)$ potential in Figure 9 (i.e. transitions to the $v_3 = 0$ level of [ClHCl]) will yield a broad peak with a width determined, to first order, by the slope of the adiabatic potential in the Franck-Condon region.

The simulation of the experimental spectrum requires solving eq 10 and 11 and calculation of Franck-Condon factors. Equation 10a is solved to obtain $\theta_{v_3'}(z;\rho)$ at 60 values of ρ , using a relaxation algorithm⁵² that takes advantage of the observation that $\theta_{v_3'}(z;\rho)$ varies slowly with ρ . If the adiabatic potential supports resonances, wave functions are found variationally.⁵³ Two-dimensional overlap integrals (12) are calculated for each state. For the repulsive region of each adiabatic potential, continuum wave functions and Franck-Condon factors are determined at an energy spacing of 1–4 meV, depending on the steepness of the adiabatic potential. The continuum Franck-Condon factors are energy-normalized by forcing the asymptotic amplitude of the outgoing wavefunction $R_{v_3'}(\rho)$ to be⁵⁴

$$P = 0.27844(m/E)^{1/4} \quad (13)$$

where m is as in eq 8, E is the energy above the asymptote, and P has units of $(\text{cm}^{-1} \text{Å})^{-1/2}$. Calculation of Franck-Condon factors as a function of energy⁵⁵ then gives Franck-Condon factors in units of $(\text{cm}^{-1})^{-1}$. Multiplication by the instrumental resolution (in cm^{-1}) gives a dimensionless intensity that can be compared directly with that derived for a bound state.

3. Application to Cl + HCl. We have simulated the ClHCl⁻ photoelectron spectra with our "effective" collinear approach using the ionic equilibrium distance and vibrational frequencies in Table II and the BCMR LEPS surface. The ions are assumed to be in their ground vibrational state. Figure 10 shows the simulated ClHCl⁻ spectrum, convoluted with our experimental resolution (eq 2). The dashed lines are the results for $v_2' = 0$ in the neutral

complex. The dotted lines represent the contribution from $v_2' = 2$, the lowest bend-excited state of the complex that has nonzero overlap with the ion ground state. The bending corrections in eq 7, $\epsilon_0(\rho, z)$ and $\epsilon_2(\rho, z)$, are calculated in a harmonic approximation.

The $v_2' = 0$ simulation shows a broad (fwhm = 35 meV) peak at high electron energy, due to overlap of the ion vibrational wave function with the continuum wave functions supported by the repulsive $U_0(\rho)$ adiabatic curve. The narrow peak at 0.74 eV is due to a transition to the long-lived shape resonance supported by the $v_3' = 2$ adiabatic curve. The $v_3' = 4$ adiabatic curve supports a Feshbach resonance (at 0.489 eV) and two shape resonances (at 0.452 and 0.424 eV). This simulation is essentially identical with one obtained by Bowman,⁵⁶ who calculated the Franck-Condon overlap with the exact two-dimensional scattering wave functions supported by the same effective collinear surfaces, again assuming $v_2' = 0$. The considerably smaller contribution from $v_2' = 2$ mimics the $v_2' = 0$ simulation with all the peaks shifted to slightly lower electron kinetic energy.

We can further test our analysis by comparing our results to the full three-dimensional simulations (with $J = 0$) recently reported by Schatz.³⁹ In his calculation, Schatz simulated the ClHCl⁻ photoelectron spectrum between 1.1 and 0.6 eV of electron kinetic energy using the BCMR LEPS surface. Our peak positions in this energy range, which includes the broad $v_3' = 0$ peak and the narrow $v_3' = 2$ peaks, agree well with Schatz' calculation. The broad peak is slightly wider (50 meV) in Schatz' simulation. The width of the resonance peaks in both simulations is determined by the experimental resolution. The $v_3' = 0$ peak in our calculation is noticeably larger relative to the resonance peaks. Schatz calculated the intensity of the $v_3' = 0$ peak at only two energies, and with a finer energy grid the appearance of this peak in his simulation might be different. The three-dimensional simulations by Gazdy and Bowman^{40b} do in fact show a more intense $v_3' = 0$ peak. These comparisons suggest that our simple model yields reasonable results for a three-dimensional potential energy surface with a collinear minimum energy path.

All of the above methods of simulation yield peaks that are much narrower and somewhat more widely spaced than the experimental peaks. Based on our experience in fitting the BrHBr⁻ and BrDBr⁻ spectra, these discrepancies can be explained in terms of possible deficiencies in the Cl + HCl model potential energy surface (see section 4C, below). We point out, however, that even the three-dimensional simulations are restricted to $J = 0$ and do not include the possibility of transitions to low-lying electronic states of [ClHCl]; these restrictions may lead to overly narrow peaks in the simulated spectra.

4. Br + HBr Potential Energy Surface. We wish to construct an "effective" collinear potential energy surface for the Br + HBr reaction and reproduce the experimental photoelectron spectra. This section discusses the connection between the experimental spectra and qualitative features of the surface, the construction of the surface, and an evaluation of the uniqueness of the surface within the assumptions made in our analysis.

A. Contributions from Resonances and Direct Scattering. The development of an appropriate potential energy surface is aided by knowing which peaks result from transitions to repulsive adiabatic potentials and which come from adiabatic potentials with wells which can support shape or Feshbach resonances. Consider the $v_3' = 0, 2,$ and 4 peaks in the BrHBr⁻ spectrum and the $v_3' = 0, 2, 4,$ and 6 peaks in the BrDBr⁻ spectrum. The $v_3' = 4$ BrHBr⁻ peak and the $v_3' = 6$ BrDBr⁻ peak are substantially narrower than the other peaks. Based on the peak widths alone, it is tempting to assign the narrow peaks as transitions to resonance states and the broad peaks to direct scattering. This assignment is supported by comparing the energy of each v_3 peak to the energy of the Br + HBr($v_3/2$) asymptotic level. Figure 5 and Table I show that the broad peaks lie above their respective asymptotic levels (at lower electron kinetic energy), while the $v_3' = 4$ peak in the BrHBr⁻ spectrum and the $v_3' = 6$ peak in the BrDBr⁻ spectrum result from transitions to states that lie just below the

(52) Press, W. H.; Flannery, B. P.; Teukolsky, S. A.; Vetterling, V. T. *Numerical Recipes*; Cambridge University Press: Cambridge, England, 1986.

(53) Shore, B. W. *J. Chem. Phys.* 1973, 58, 3855.

(54) Tellinghuisen, J. *Adv. Chem. Phys.* 1985, 60, 299.

(55) LeRoy, R. J. *University of Waterloo Chemical Physics Research Report CP-329*, 1988.

(56) Bowman, J. M., private communication.

TABLE IV: Parameters for the Fitted Br + HBr Potential^a

$R_{\text{Br-Br}}, \text{\AA}$	$x_1, \text{\AA}$	$b, \text{kJ/mol}$	$h, \text{kJ/mol}$	$k, [(\text{kJ/mol})/\text{\AA}^2]$	$q, [(\text{kJ/mol})/\text{\AA}^4]$
2.6	0.0	-50.0	0.0	5.0	1.3
2.8	0.0	-140.0	0.0	4.0	1.6
3.0	0.0	-215.0	0.0	2.9	2.1
3.29	0.0	-330.5	0.0	0.8	2.0
3.4	0.31	-343.5	15.0	1.6	18.0
3.5	0.465	-360.5	33.5	1.1	62.0
3.6	0.541	-370.0	51.0	0.8	22.0
3.7	0.613	-374.9	84.0	0.9	6.0
3.85	0.719	-376.8	135.0	1.0	2.2
4.0	0.826	-377.0	170.0	1.05	1.2
4.2	0.968	-377.1	217.0	1.08	0.9
4.7	1.322	-377.3	300.0	1.23	0.3

^aThe form of the potential is eq 6, for each value of $R_{\text{Br-Br}}$. The global potential is defined by connecting the parameters with natural cubic splines at the values of $R_{\text{Br-Br}}$ given in the table. For x_1 and h , the smallest spline point is $R_{\text{Br-Br}} = 3.29 \text{\AA}$.

Br + HBr($v=2$) and Br + DBr($v=3$) levels, respectively. Each broad peak then results from a transition to a region of an adiabatic potential curve that lies above the asymptotic limit of the curve. Such a transition will occur if the adiabatic potential is purely repulsive, in which case the broad peak can be attributed to direct scattering. Each narrow peak appears to result from a transition to a region of an adiabatic potential that lies below its asymptotic limit. This means the potential *must* have a well, which is the necessary condition for the existence of Feshbach resonances.

Unfortunately, the 0.05-eV uncertainty in the bond dissociation energy for BrHBr⁻ is comparable to the energy differences between the narrow peaks and the relevant asymptotic levels. For example, the $v_3' = 6$ BrDBr⁻ peak could result from a transition to a state that lies 0.04 eV above the Br + DBr($v=3$) level. This peak could therefore arise from a shape resonance or from a transition to a very flat repulsive curve. In any case, the assignment of the broad peaks to direct scattering and the narrow peaks to resonances is supported by the narrowing of peak widths in the energy range where resonances might be expected.

These considerations are useful in constructing a Br + HBr potential energy surface. On the correct surface, the U_0 and U_2 (and, for Br + DBr, U_4) adiabatic potentials should be repulsive in the Franck-Condon accessible range of ρ , while the Br + HBr U_4 and Br + DBr U_6 potentials should each have a well or be very flat in this region. This information is helpful, because it is easier to visualize the effect of varying the potential energy surface on the adiabatic potentials than on the full simulation of the photoelectron spectrum.

B. Functional Form for the Potential Energy Surface. We next choose a flexible functional form for the potential energy surface, using adjustable parameters that can be optimized to reproduce the experimental photoelectron spectra. Our one-dimensional analysis indicates that a double minimum potential given by eq 6 is appropriate for the antisymmetric stretch potential at fixed ρ . A two-dimensional potential energy surface $V(\rho, z)$ is then constructed by smoothly connecting a series of one-dimensional potentials $V(z)$ at various values of ρ . Each one-dimensional potential represents a cut through the effective collinear surface along the z direction at a constant value of ρ . For convenience, we use the mass-independent coordinates $R_{\text{Br-Br}}$ and $x = (R_{\text{Br-H}} - R_{\text{H-Br}})/2^{1/2}$ for the potential energy surface. The resulting two-dimensional function $V(R_{\text{Br-Br}}, x)$ is then converted to the (mass-weighted) hyperspherical coordinates ρ and z so that $V(\rho, z)$ may be substituted in the differential equations (10). The equations for the one-dimensional potentials are those in eq 6, except that the potential parameters (b, h, x_1, k, q) depend on the inter-bromine distance $R_{\text{Br-Br}}$. The potentials have a single minimum for $R_{\text{Br-Br}} < R_{\text{Br-Br}}$ (saddle point) and two minima at higher values of $R_{\text{Br-Br}}$. The potential parameters are defined at 12 values of $R_{\text{Br-Br}}$ (see Table IV) and are interpolated by using natural cubic splines to form a smooth potential. The saddle point is specified by the largest value of $R_{\text{Br-Br}}$ for which $x_1 = 0$; the

barrier is then $b(R_{\text{Br-Br}} = \text{saddle point}) - b(R_{\text{Br-Br}} = \text{infinity})$. The variation of b with $R_{\text{Br-Br}}$ specifies the energy along the minimum energy path; the steepness of the minimum energy path can easily be varied and strongly affects the simulated peak widths.

This form of the potential energy surface is completely empirical. It does not automatically predict the characteristic frequencies of reactants and products at the asymptotes. In the asymptotic region ($R_{\text{Br-Br}} \geq 4.7 \text{\AA}$), the location of the minimum in the product valley approaches the limiting value

$$x_1 = (1/2^{1/2})(R_{\text{BrH}} - R_e(\text{HBr})) = (1/2^{1/2})(R_{\text{Br-Br}} - 2R_e(\text{HBr})) \quad (14)$$

where $R_e(\text{HBr})$ is the bond length in HBr (1.4144 \AA). The remaining parameters are then set to approximate the vibrational frequency and anharmonicity of HBr.

Equation 14 is important in the fitting procedure, since it provides an upper bound to x_1 for any value of ρ (or $R_{\text{Br-Br}}$). A larger value of x_1 in this region means that the HBr bond shortens as the Br atom approaches in a Br + HBr reactive collision. This runs counter to chemical intuition, which suggests that the HBr bond weakens and lengthens as the Br approaches. Thus, a physically reasonable potential energy surface should have x_1 below the limit given by eq 14, and near the saddle point x_1 should be substantially less than the bound given by (14). (Note that $x_1 = 0$ at the saddle point.)

Although the potential energy function given above has a large number of parameters, the goal of this analysis is to establish the existence of an "effective" collinear potential energy surface that reproduces the experimental BrHBr⁻ and BrDBr⁻ spectra. It is likely that a simpler functional form employing fewer, more physically meaningful, parameters could be used successfully, and this is a subject for future analysis of this system.

C. Results of the Analysis. The potential energy surface that provides the best fit to the experimental results is shown in Figure 11. Simulated and experimental spectra corresponding to this surface are shown above the potential energy surface. For both BrHBr⁻ and BrDBr⁻, the experimental peak positions, intensities, and widths for the ground-state progression are generally reproduced in the simulations. Because of our experience with Cl + HCl, we expended most effort on fitting the peak positions. The accuracy of the simulated peak widths and intensities is less certain, particularly for the peaks due to direct scattering. The high-energy "tail" on the $v_3' = 0$ peaks in the experimental spectra is probably due to ions with some excitation in the low-frequency v_1 mode; the simulations assumed $v_1 = v_3 = 0$ in the ion. Transitions to the electronically excited [BrHBr]^{*} state are not included in this analysis.

The simulations in Figure 11 assume that the equilibrium inter-bromine distance R_e in BrHBr⁻ is 3.50 \AA . Attempts to fit the spectra using the ab initio R_e of 3.43 \AA ⁴³ resulted in a potential energy surface that did not satisfy eq 14. Our assumed value is within the error bars of the ab initio calculation and greatly facilitated fitting the data to a reasonable potential energy surface. However, our analysis is quite sensitive to the assumed value of R_e . It is clear that the accurate experimental determination of the anion R_e would provide an important constraint in the construction of the Br + HBr potential energy surface. The experimental approach most likely to yield this value is velocity-modulated infrared spectroscopy of the ion,⁵⁷ which should result in a rotationally resolved spectrum from which R_e can be obtained. This method has been used to determine R_e for FHF⁻ and ClHCl⁻.

The parameters for our potential energy surface are given in Table IV. This potential energy surface has a saddle point at $R_{\text{Br-Br}} = 3.29 \text{\AA}$ and a barrier of 46.8 kJ/mol along the minimum energy path. This potential is the effective collinear surface $V(\rho, z)$ in eq 7, which implicitly includes the bending zero-point energy. Our analysis does *not* divide $V(\rho, z)$ into a collinear and bending contribution, as this would require assuming the form of the bending potential. We estimate the bending zero-point energy

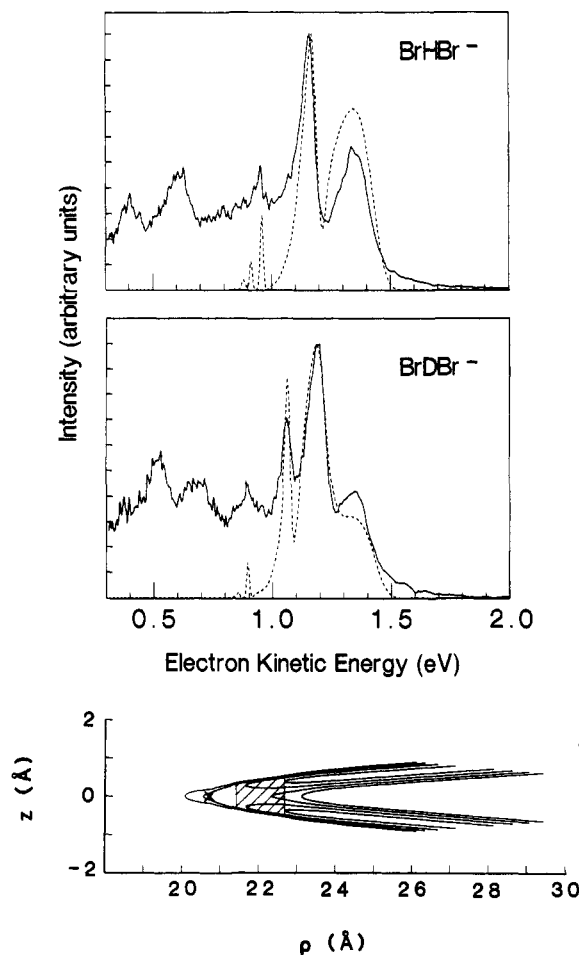


Figure 11. (top) Simulated photoelectron spectra of BrHBr^- and BrDBr^- using our best fit $\text{Br} + \text{HBr}$ effective collinear surface. The simulated spectra (---) have been convoluted with the experimental resolution (eq 2) and are superimposed on the experimental spectra. (bottom) Contour plot of the best fit effective collinear potential energy surface for the $\text{Br} + \text{HBr}$ reaction. For $\text{Br} + \text{HBr}$, $z \approx 1/2(R_{\text{BrH}} - R_{\text{HBr}})$ and $\rho \approx 6.30R_{\text{Br-Br}}$. The saddle point is at $R_{\text{Br-Br}} = 3.29 \text{ \AA}$; $\rho = 20.72 \text{ \AA}$. The Franck-Condon region is shaded. Contours are at -300 , -325 , -350 , and -370 kJ/mol with respect to three-atom dissociation. The parameters for the surface are given in Table IV.

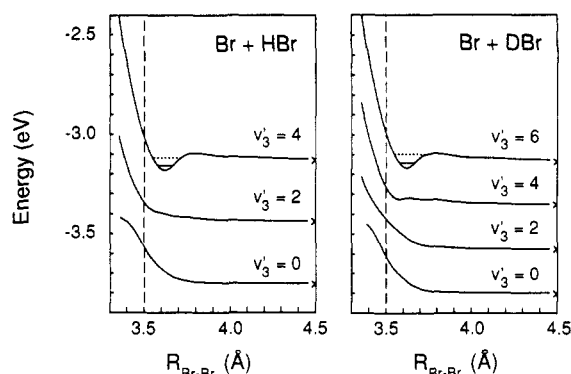


Figure 12. Adiabatic curves $U_{v_3}(\rho)$ for $\text{Br} + \text{HBr}$ and $\text{Br} + \text{DBr}$ on the surface shown in Figure 11. Shape resonances are denoted by dotted lines and Feshbach resonances by solid lines. The asymptotic levels of $\text{Br} + \text{H(D)Br}$ ($v = v_3/2$) are denoted by arrows. The dashed line is drawn at the value of R_c for BrH(D)Br^- used in our analysis (3.5 \AA).

at the saddle point to be 4–8 kJ/mol on the basis of model $\text{Cl} + \text{HCl}$ surfaces, so the saddle point energy for the collinear BrHBr geometry is approximately 40 kJ/mol. This is considerably higher than the barriers on previously proposed model potential energy surfaces for the $\text{Br} + \text{HBr}$ reaction.^{38b,58} The adiabatic potentials

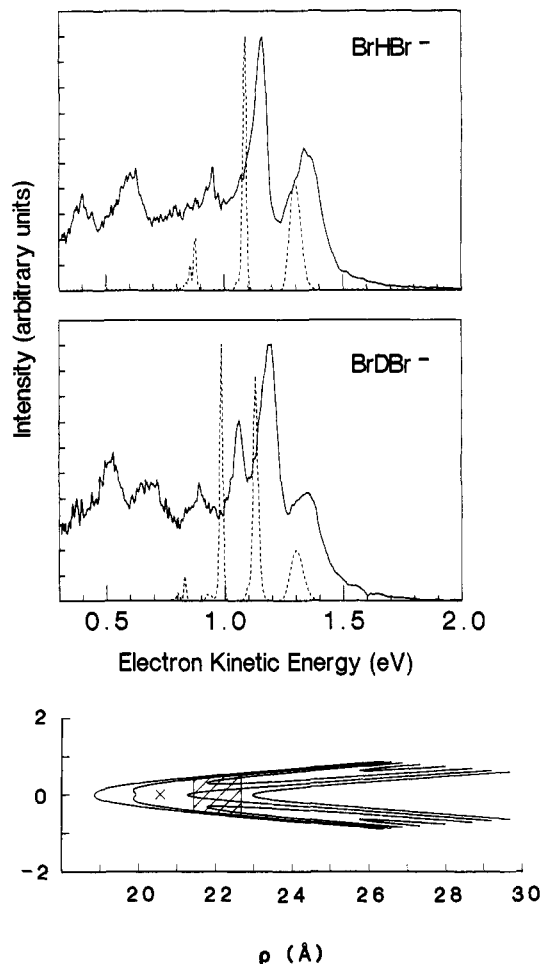


Figure 13. (top) Simulated photoelectron spectra of BrHBr^- and BrDBr^- (---) using LEPS surface for $\text{Br} + \text{HBr}$ shown at bottom of figure. The simulated spectra have been convoluted with the experimental resolution (eq 2) and are superimposed on the experimental spectra. (bottom) Contour plot of LEPS potential energy surface (including zero-point bend) for $\text{Br} + \text{HBr}$ with barrier and saddle point very similar to that of the surface in Figure 11. Contours are at -300 , -325 , -350 , and -370 kJ/mol with respect to three-atom dissociation. The parameters for the surface are given in Table V.

for the first few v_3' levels of $\text{Br} + \text{HBr}$ and $\text{Br} + \text{DBr}$ are shown in Figure 12. The U_4 ($\text{Br} + \text{HBr}$) and U_6 ($\text{Br} + \text{DBr}$) curves each have a shallow well that supports resonance states; the lower curves are purely repulsive.

We next consider the uniqueness of our potential energy surface. We divide the surface into four ranges of ρ . In order of increasing ρ , these are (i) the saddle point region, which includes the saddle point and the repulsive wall at small ρ , (ii) the Franck-Condon region, (iii) the intermediate region, between the Franck-Condon region and the asymptotic region, and (iv) the asymptotic region (large ρ). Region iv depends on the asymptotic properties of $\text{Br} + \text{HBr}$, which are well characterized. The requirement that the potential energy surface vary smoothly from the Franck-Condon region to the asymptotic region constrains the parameters that specify the intermediate region, although our study is not sensitive to features of the surface (such as van der Waals wells) that occur in this range. Our experiment is most sensitive to features of the surface in the Franck-Condon region, and least sensitive to the saddle point region. The saddle point parameters are extrapolations from better-determined regions of the surface, but as mentioned above, the Franck-Condon region of the surface is likely to be more important than the saddle point region in the dynamics of this reaction.

To further illustrate the sensitivity of our experiment to the nature of the potential energy surface, the BrHBr^- and BrDBr^- spectra have been simulated by using an effective collinear surface derived from a three-dimensional LEPS surface, assuming $v_2' =$

(58) White, J. M.; Thompson, D. L. *J. Chem. Phys.* **1974**, *61*, 719.

TABLE V: Parameters for the Br + HBr LEPS Potential

parameter	HBr	Br ₂
D_e , kJ/mol	387.3	192.1
r_e , Å	1.4144	2.281
b , Å ⁻¹	1.810	1.964
S	0.075	0.075

^aThe "effective" collinear potential has a barrier of 48.65 kJ/mol at $R_{\text{Br-Br}} = 3.266$ Å.

0 in the complex. The barrier height and saddle point geometry on this effective collinear surface are similar to our "best fit" surface. The LEPS simulations, shown in Figure 13, are clearly inferior. The peaks are shifted to low electron kinetic energy, suggesting that the minimum energy path in the Franck-Condon region lies too far above the asymptote. In addition, the peak spacings are too large, the peaks are too narrow, and the intensities are incorrect.

If we take one-dimensional cuts at constant ρ through the Franck-Condon region of each surface, we obtain antisymmetric stretch potentials that are similar to those shown in Figure 7 for the Cl + HCl reaction; the outer walls are not as steep on our surface, and the two minima in the potential are further apart than those of the LEPS surface. This explains the differences in the simulated peak positions and intensities for the two surfaces. In addition, the minimum energy path on our surface begins to rise later in the course of the reaction (i.e., at smaller values of ρ). For equal barrier heights, the minimum energy path is steeper in the Franck-Condon region on our surface, resulting in adiabatic potentials that are more repulsive in the Franck-Condon region and peaks that are substantially broader. Since the effective collinear surfaces used in these simulations include the bending zero-point energy, we cannot say whether the later rise in the minimum energy path on our surface is due to differences in the bend potential or in the collinear electronic interaction between the reactants. This comparison shows that reactive surfaces with similar saddle point properties can give very different simulated spectra.

The discrepancies between the simulated and experimental results for ClHCl⁻ are similar to the differences between the BrHBr⁻ LEPS simulation and experimental results. These can be explained in terms of possible defects in the Cl + HCl LEPS surface similar to those found for the LEPS surface in Figure 13. The barrier height on the LEPS surface used in the ClHCl⁻ simulations is consistent with ab initio calculations and experimental results on the Cl + HCl reaction. However, the BrHBr⁻ analysis suggests that the Cl + HCl LEPS surface is too flat in the Franck-Condon region and that an effective collinear surface having the same barrier height, but sharing more of the features

of our Br + HBr surface, would better reproduce the experimental results.

Summary and Conclusions

The photoelectron spectra of the negative ions ClHCl⁻, BrHBr⁻, and their deuterated analogues provide a sensitive probe of the transition-state region of the Cl + HCl and Br + HBr reactions. The spectra show progressions in the antisymmetric stretch vibration of the neutral [ClHCl] and [BrHBr] complexes. The observed peak widths are an indication of the dissociation dynamics of the complexes. The BrHBr⁻ and BrDBr⁻ spectra exhibit broad peaks assigned to directly dissociating states of the neutral complex, narrow peaks assigned to reactive resonance states, and peaks that appear to originate from electronically excited states of the complex. We have analyzed the spectra by assuming that the reactions under study are governed by effective collinear potential energy surfaces. For the Br + HBr reaction, a flexible functional form for such a surface has been developed, and we have found a set of parameters that allows us to simulate the peak positions, widths, and intensities in the experimental BrHBr⁻ and BrDBr⁻ photoelectron spectra.

We plan to study these ions with our high-resolution (0.3 meV) threshold photodetachment spectrometer³² to more accurately determine the positions and widths of the resonance peaks. Our results also suggest avenues for further theoretical work on these systems. The validity of the effective collinear surface determined here for the Br + HBr reaction could be tested with more accurate simulations using full three-dimensional potential energy surfaces that yield our surface in the reduced dimensionality model. Accurate simulations on potential energy surfaces with bent transition states, for which the effective collinear approximation is inappropriate, will also be of interest. It will be useful to see if other types of semiempirical potential energy surfaces (such as a DIM surface) are more successful than a LEPS surface at reproducing our experimental results. Finally, it is worthwhile to examine how sensitive the asymptotic properties of the Br + HBr reaction are to the regions of the potential energy surface which are well-characterized by our experiment.

Acknowledgment. This research is supported by the Air Force Office of Scientific Research under Contract No. AFOSR-87-0341. D.M.N. thanks the Camille and Henry Dreyfus Foundation for a Distinguished New Faculty grant. Additional support from the Research Corporation and the donors of the Petroleum Research Fund, administered by the American Chemical Society, is gratefully acknowledged. We thank George Schatz and Joel Bowman for many stimulating discussions.

Registry No. Cl, 22537-15-1; HCl, 7647-01-0; Br, 10097-32-2; HBr, 10035-10-6.